STUDENT JOURNAL OF PHYSICS

Pion Decay Constant from Lattice QCD

Quintin E. Muhlenkamp [1**]

[1] Junior, Department of Physics, Wittenberg University, Springfield, Ohio, USA, 45504

Date Received: 31/Oct/2019 **Date Published: 21/Aug/2020**

Abstract. We present results for the value of the pion decay constant f_π, needed for understanding weak pion decay. We analyze lattice-QCD data from six ensembles generated by the MILC collaboration. Lattice spacings of $a \approx 0.06$, 0.09, and 0.12 fm are used, along with pion masses of $m_\pi \approx 130$, 220, and 310 MeV. Statistical errors are quantified and accounted for using jackknife resampling. Using a ground-state fit, the mass and decay constant are estimated for each ensemble. These estimates are then used to extrapolate the decay constant to the physical point. This procedure yields $f_\pi = 103.5(4.5)$ MeV with no QED correction and $102.7(4.7)$ MeV in the chiral limit.

Keywords: Pion Decay Constant, Lattice QCD

1. INTRODUCTION

The pion decay constant f_π is a multiplicative term used to describe the coupling of the charged pion to the mediating W boson in weak decay. The constant's precise value is important for checking a unitarity constraint on the Cabibbo-Kobayashi-Maskawa (CKM) matrix, which describes the inter-generational mixing of quark flavor. If f_π is known with small enough uncertainty, along with the kaon decay constant f_K, the matrix element V_{us} can be precisely determined, giving us insight into the possibility of new physics beyond the Standard Model. To improve the precision of the matrix element, we need theoretical work to decrease the uncertainty associated with its calculation. The goal of this work is, therefore, to use state-of-the-art lattice-QCD calculations to determine f_π and compare with other theoretical values.

Lattice QCD is a nonperturbative numerical technique used to investigate the properties of hadrons. Lattice must be used because of the complexity of the QCD vacuum associated with the Goldstone pion. Rather than an empty vacuum we would expect classically, the QCD vacuum introduces topological charge and the effects of chiral symmetry breaking that restrict the use of perturbative methods. Lattice QCD discretizes four-dimensional Euclidean space, then solves path integrals over configurations that are placed onto the lattice. During the discretization, a lattice of spacing a is laid over the hypercube, where vertices hold the quarks, and the connections hold the gluons. Data is then extracted with a correlation function, designed to work specifically with

** muhlenkampq@gmail.com

the set of lattice data. A correlation function contains operators at two points in spacetime and describes the evolution of a state from its source to sink [1]. The lattice gauge configurations of $N_f = 2 + 1 + 1$ were computed by the MILC collaboration [2]. The correlation functions were constructed by the PNDME collaboration [3]. To improve the distinction between the ground and excited states, the lattice operators are smeared. Smearing is equivalent to describing a hadron with a state created by an operator of nonzero spatial extent, rather than by a point. An example could be stretching the point into the shape of a gaussian distribution. This procedure helps improve the overlap of the creation and annihilation operators with the hadronic state of interest. Lattice QCD introduces deviations from the physical world such as discrete space and non-physical pion masses (used for computational convenience). However, these values can be extrapolated to physical ones as explained in the methodology.

2. METHODOLOGY

This work looks at two different types of smeared data. The first has both the source and sink smeared and is referred to as smear-smear; its correlation function looks like:

$$C_s(t) \approx \frac{Z_s^2}{2am_\pi} e^{-am_\pi t} = A_s e^{-am_\pi t} \tag{1}$$

where $C_s(t)$ is the correlator for the smear-smear dataset, Z_s is a measurement of the amount of overlap between the smeared operator and the pion ground state, t represents the number of time-steps between the source and sink, and am_π is the mass of the pion in lattice units. It should be noted that $\frac{Z_s^2}{2am_\pi}$ can be written as the smear-smear amplitude A_s, which is a parameter used in the fitting procedure. The other type of smearing used is local-axial, which smears only one component:

$$C_a(t) \approx \frac{Z_s}{2am_\pi} \langle \pi | \mathscr{A}_t | 0 \rangle \, e^{-am_\pi t} = A_a e^{-am_\pi t} \tag{2}$$

where $C_a(t)$ is the local-axial correlator, $\langle \pi | \mathscr{A}_t | 0 \rangle$ is the axial-current matrix element, and $\mathscr{A}_t$ is the axial current $\overline{q}\gamma^5 q$, where $\overline{q}$ is an antiquark, q a quark, and γ^5 represents the product of all gamma matrices. $\langle \pi | \mathscr{A}_t | 0 \rangle$ is a constant proportional to f_π through the relation

$$\langle \pi | \mathscr{A}_t | 0 \rangle = f_\pi^{\text{bare}} m_\pi, \tag{3}$$

where f_π^{bare} is the pion decay constant before renormalization, and m_π is the pion mass.

Because we are ultimately interested in finding $\langle \pi | \mathscr{A}_t | 0 \rangle$, its plots need particular attention. The shape of this plot changes between datasets, as do the others, but is unique because it cannot be found directly from fitting $C_s(t)$ and $C_a(t)$ independently. From Eq. 2 one can see that the ground-state fit will yield am_π and A_a. The constant $\langle \pi | \mathscr{A}_t | 0 \rangle$ can then be solved for if Z_s is known from a fit of $C_s(t)$. This method of finding $\langle \pi | \mathscr{A}_t | 0 \rangle$, referred to as Method I, is compared to another method to determine the most stable approach. Method II requires one fit of a manipulated correlator:

$$\frac{C_a(t)^2}{C_s(t)} \approx \frac{\langle \pi | \mathscr{A}_t | 0 \rangle^2}{2am_\pi} e^{-am_\pi t} = A_r e^{-am_\pi t} \tag{4}$$

where am_π and A_r is the mass and amplitude of the manipulated correlator, respectively. By comparing the $\langle\pi|\mathscr{A}_t|0\rangle$ evolution plots for these two methods we can determine which is better suited for finding the constant. Figure 1 shows a plot of the fitted matrix element as a function of t_{min}, the minimum time used in the fit, for both methods. The manipulated correlator is slightly less stable because it is constantly increasing; for this reason all values of $\langle\pi|\mathscr{A}_t|0\rangle$ were found using Method I.

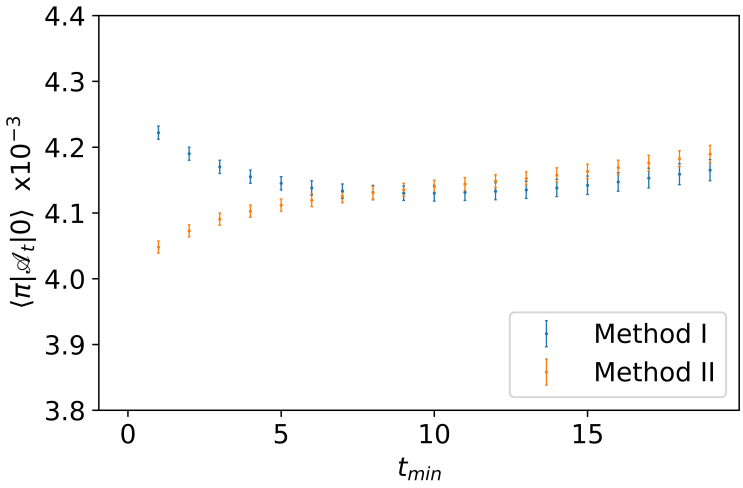

Figure 1. The constant $\langle\pi|\mathscr{A}_t|0\rangle$ as a function of minimum fit time for both fit methods of the a06m310 ensemble. Because the result from Eq. 4 (orange markers) is always increasing, it was deemed less stable than the method requiring a fit of each the $C_s(t)$ and $C_a(t)$ correlators from Eq. 1 and Eq. 2, respectively (blue markers).

The constant $\langle\pi|\mathscr{A}_t|0\rangle$ can be extracted from the correlator data using an uncorrelated ground-state fit. The ground-state fit looks like a single exponential term where the two parameters are the amplitude and energy of the pion at its lowest energy state. Because the lowest-energy state is at rest, the energy parameter is the mass. Therefore, on a plot of effective mass a good correlator fit will also fit the effective-mass plateau, where the pion is at its ground-state energy. The effective mass is given by

$$m_{\text{eff}} = \ln\left(\frac{C(t)}{C(t+1)}\right), \tag{5}$$

where $C(t)$ is any correlator. The effective-mass plot is a valuable tool in fitting the correlator, as it provides easy visualization of the ground state and allows us to easily see whether there is higher-state contamination. We fit jackknifed correlator data to reduce bias. Because we only want to fit the ground state, a minimum and maximum time of the fit needs to be designated so that any points that pull the data away from the ground state are removed. These limits are chosen based on the evolution of the fitting parameters, $\langle\pi|\mathscr{A}_t|0\rangle$, and the $\frac{\chi^2}{\chi^2_{\text{min}}}$ with increasing t_{min} and decreasing

t_{max}, the maximum time used in the fit (Fig. 2). When the higher state is completely removed these evolution plots appear stable, showing little to no change in the magnitude of the parameter with changing t_{max} or t_{min}. The effective-mass plot is also consulted, as there may appear many possible bounds in the evolution plots, the effective mass aids in determining a good fit.

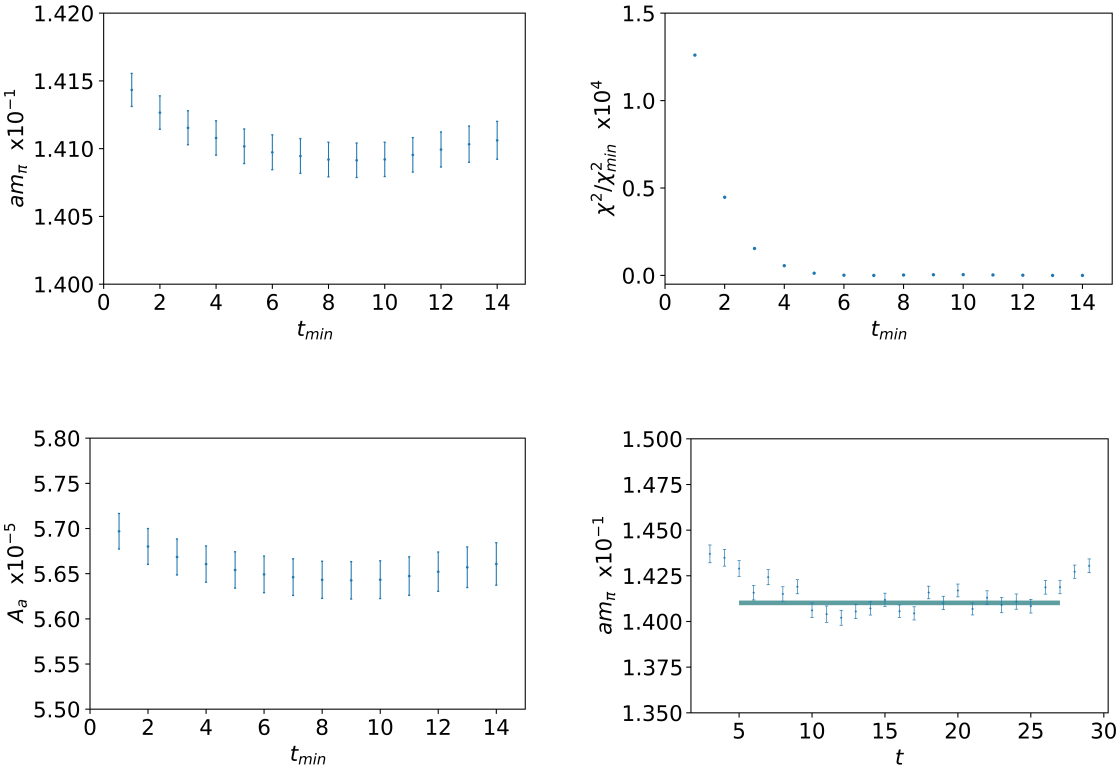

Figure 2. t_{min} evolution plots, and ground-state fit for the a09m310 ensemble. (Top left) Mass parameter in lattice units (am_π) changing with increasing t_{min}. (Top right) Chi squared approaches one as t_{min} increases. (Bottom left) The amplitude evolution with t_{min}. (Bottom right) The correlator fit band shown on the effective-mass plot as a function of time. Uncertainty is given as the width of the band. The minimum time is chosen to be in a region that is relatively stable, for this ensemble $t_{\text{min}} = 5$ to $t_{\text{min}} = 10$ was considered stable, in this case $t_{\text{min}} = 5$ was chosen to fit the most data. t_{max} is determined in a similar manner.

3. RESULTS AND DISCUSSION

The pion mass in lattice units am_π is taken from the effective-mass plot and converted into physical units m_π for use in Eq. 3. The bare pion decay constant f_π^{bare} can then be renormalized to the pion decay constant f_π (Table 1) using a renormalization constant Z_A found in Ref. [3]. The results from the fit of all six ensembles are found in Table 1.

Ensemble	Z_A	a **(fm)**	m_π **(MeV)**	f_π **(MeV)**	$L^3 \times T$
a12m310	0.95(3)	0.1207(11)	311.0(2.9)	93.3(3.5)	$24^3 \times 64$
a12m220	0.95(3)	0.1184(10)	288.5(2.0)	95.8(3.6)	$32^3 \times 64$
a09m310	0.95(4)	0.0888(08)	312.8(2.8)	98.3(4.6)	$32^3 \times 96$
a09m220	0.95(4)	0.0872(07)	226.6(1.8)	95.8(4.4)	$48^3 \times 96$
a09m130	0.95(4)	0.0871(06)	142.5(1.0)	93.9(4.2)	$64^3 \times 96$
a06m310	0.97(3)	0.0582(04)	319.5(2.2)	101.9(3.5)	$48^3 \times 144$

Table 1. The renormalization constant Z_A and lattice spacing a for each ensemble [3], along with the fit results for pion mass m_π and decay constant f_π with their respective statistical errors. The far right column labels the lattice sizes along the spatial (L) and temporal (T) directions.

The results from the correlator fits cannot yet be compared to the physical value because of the non-physical assumptions made during the lattice calculation. The lattice spacing and pion mass must be extrapolated to their physical values. Using the fit function [3, 4]:

$$f(a, m_\pi) = C_0 + C_a a + C_m m_\pi^2, \tag{6}$$

the correlator results can be fit to a plane and the physical value interpreted from this relationship. The f_π mean and error associated with every ensemble are recreated using the jackknife mean and variance of a randomly generated gaussian distribution. The jackknife samples are then fit with Eq. 6 and extrapolated to $m_\pi = 139.57061(24)$ [5], and $a = 0$. The pion mass and error from Ref. [5] were also reconstructed for calculation using gaussian sampling.

The extrapolation is viewed as cross sections through a three-dimensional plot so that the dependence of f_π on a and m_π can be viewed independently (Fig.3). When extrapolated to the physical point the fit of the ensemble data (Table 1) to Eq. 6 yields a value of $f_\pi = 103.5(4.5)$ MeV.

Compared to the accepted experimental value of 89.80 (1)(9), the errors come from the experimental rate measurement and the radiative correction factor, respectively [5], our value is slightly large. The difference is less substantial when compered to other lattice calculations such as the value found in Ref. [3] of approximately 95 MeV. This may be the result of higher-state contamination left over from the correlator fit. The ground-state fit exposes the mass to the possibility of higher-state influence. Although the fitting procedure aims to fit only the effective-mass plateau, the possibility of higher-state influence is not completely eliminated, as the plateau is not always clearly defined. In

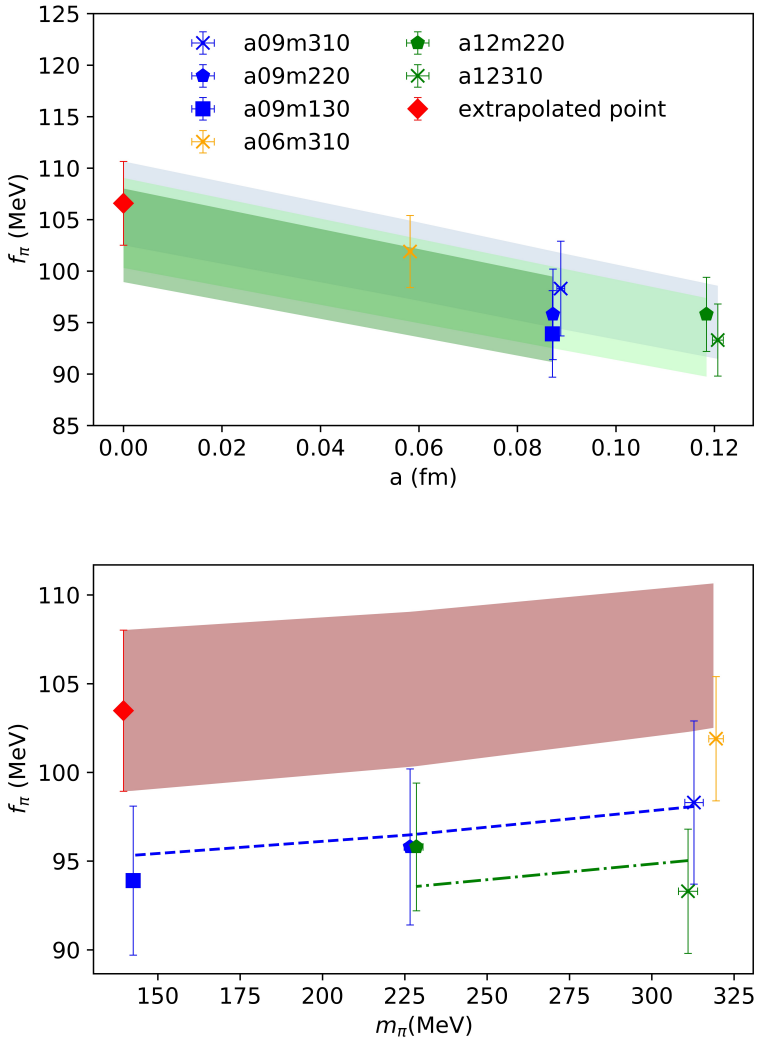

Figure 3. (Top) Final decay-constant fits for all three masses when extrapolated to the continuum limit as a function of lattice spacing. This is a slice along the mass domain of the three-dimensional plot generated from Eq. 6. The masses are distinguished by the marker shape, while the lattice spacing by marker color. The red marker is the value of f_π at the continuum. The trend shows that f_π decreases with increasing a. The dependence of f_π on the mass is also visible by the stacking of the fit bands, greater mass yields a greater f_π. These relationships are again confirmed when observing f_π versus m_π (bottom), which is a slice along the lattice-spacing domain. It is obvious that f_π depends heavily on a.

future work, contamination could be eliminated by using a higher-state fit, accomplished by adding another exponential term onto the fit function. By including the higher-energy states, there is less chance of outside contamination during the fit. This analysis also provides values for C_a, C_m, and the chiral limit C_0 (Table 2). These constants provide additional insight into quark behavior.

	Fit Results	**Units**
C_0	102.7 (4.7)	MeV
C_a	–94.2 (3.9)	MeV $\cdot$ fm^{-1}
C_m	$3.78(0.64) \times 10^{-5}$	MeV^{-1}
f_π	103.5 (4.5)	MeV

Table 2. Results from the fit of ensemble data using Eq. 6, where C_0, C_a, and C_m are all constants, and C_0 is the chiral limit.

4. CONCLUSIONS

The pion decay constant provides insight into the ability of QCD to explain physics at the femtoscale (10^{-15} m). In this analysis f_π is determined from lattice-QCD ensembles generated by the MILC collaboration [2]. The value for f_π without QED correction is $f_\pi = 103.5(4.5)$ MeV, considering only statistical errors. This is slightly higher than [3, 5] which yield a value of approximately 95 MeV and 89.80 (1)(9) MeV, respectively. Future work may investigate the influence of the higher-energy states in the data. Additionally, this work could be expanded to approximate the value of the weak mixing matrix element V_{us}, providing further insight into the accuracy of QCD.

5. ACKNOWLEDGMENTS

I owe a special thanks to Professor Huey-Wen Lin, Zhouyou Fan, Rui Zhang, Ruizi Li, and Kuan-Yu Lin of Michigan State University Department of Physics and Astronomy for their guidance throughout this work. This material is based upon work supported by the National Science Foundation (NSF) under Grant No. 1559866. This work is in contribution to CAREER: Constraining Parton Distribution Functions for New Physics Searches, NSF Grant No. 1653405.

References

[1] R. Gupta, Introduction to lattice QCD: Course, arXiv:hep-lat/9807028v1
[2] A. Bazavov et al. (MILC Collaboration), Phys.Rev. D87, 054505 (2013), arXiv:1212.4768 [hep-lat].
[3] Battacharya et al. (PNDME Collaboration), Phys.Rev. D94, 054508 (2016), arXiv:1606.07049v3[hep-lat].
[4] The Flavor Lattice Averaging Group (FLAG), (2019), arXiv:1902.08191v2[hep-lat].
[5] M. Tanabashi et al. (Particle Data Group). Phys.Rev. D98, 030001 (2018) and 2019 update.